Quantum mechanical entanglements with chaotic dynamics

1996 J. Phys. A: Math. Gen. 29 5475

(http://iopscience.iop.org/0305-4470/29/17/020)

J. Phys. A: Math. Gen. **29** (1996) 5475–5497. Printed in the UK

Quantum mechanical entanglements with chaotic dynamics

Atushi Tanaka

Department of Applied Physics, Tokyo Institute of Technology, Oh-okayama, 2-12-1, Meguro, Tokyo, Japan

Received 11 October 1995, in final form 17 May 1996

Abstract. The effect of nonlinear dynamics on quantum correlations is studied by using the spin-kicked rotor, as a model system, which consists of a two-level system and a kicked rotor. Quantum-mechanical entangled states between the two-level system and the rotor form 'tunnelling' doublets when the corresponding classical dynamics of the rotor is regular. In contrast to this, chaotic dynamics of the rotor makes chaotic entangled states after the destruction of these tunnelling doublets.

1. Introduction

When we study a composite quantum system, which consists of several elements, we usually divide the system into subsystems as a description. However, for describing the system being composed of subsystems, we must pay the penalty that each subsystem is not generally in a definite state, even when the total system is in a pure state; i.e. these subsystems generally have non-classical correlations. Even if there is no quantum correlation at all in an initial state, a time evolution of the total system generally produces a state quantum-mechanically correlated between the subsystems. Such entanglements between subsystems are not only interesting phenomena themselves but also provide conceptual problems of quantum mechanics (d'Espagnat 1976, Zurek 1982). In this paper, we study the effect of nonlinear dynamics on quantum correlations. Since the Schrödinger equation is a linear equation, we use the term *nonlinearity* to the corresponding classical system, whose qualitative feature essentially determines quantal properties (Gutzwiller 1990).

A two-level system coupled to other degrees of freedom, say, a *colleague*, provides a simple model of entanglements. Here we explain how 'tunnellings' in the two-level system affects entanglements between these two subsystems. First, we start from the simplest case, an isolated two-level system $\hat{H}_{\mathrm{I}} = \epsilon\hat{\sigma}_z + J\hat{\sigma}_x$, where $\hat{\boldsymbol{\sigma}} = (\hat{\sigma}_x, \hat{\sigma}_y, \hat{\sigma}_z)$ are Pauli matrices. If we set $J = 0$, eigenvectors of $\hat{H}_{\mathrm{I}}$ are two 'localized' states $|\uparrow\rangle$ and $|\downarrow\rangle$ whose eigenvalues are $+\epsilon$ and $-\epsilon$, respectively. When we introduce non-zero 'tunnelling matrix element' J, two eigenvectors of $\hat{H}_{\mathrm{I}}$ form a pair of 'tunnelling doublets' which are linear superpositions of two localized states $|\uparrow\rangle$ and $|\downarrow\rangle$. Thus we get a model of tunnellings between two manifolds up ($\sigma_z = +1$) and down ($\sigma_z = -1$) in the two-level system. Next, we couple this two-level system to the colleague. Two different dynamics of the colleague at two manifolds $\sigma_z = +1$ and -1 destroy coherent tunnelling oscillations in the two-level system and make two subsystems entangled. Consequently, most of the tunnelling processes now become incoherent tunnelling (Kagan and Klinger 1974, Holstein 1959) in which not only the two-level system but also the colleague tunnels at once. When the difference

0305-4470/96/175475+23$19.50

of the two colleagues' dynamics is small, we can expect that the tunnelling between two manifolds is only slightly incoherent and the resultant tunnelling states still form tunnelling doublets. In our numerical experiments to investigate incoherent tunnellings we confirmed that a 'regular' colleague produces tunnelling doublets. On the other hand, we found that a 'chaotic' colleague produce chaotic entangled states, which do not compose tunnelling doublets.

This paper is organized as follows. In section 2, we introduce the spin-kicked rotor (the kicked rotor for a spin-$\frac{1}{2}$ particle (Scharf 1989)) as the target of our numerical experiments. In the numerical experiments, we evaluate the degree of entanglement by the polarization (Landau and Lifshitz 1977, section 59), which is introduced in section 3. In section 4, we show the result of our numerical experiments. In section 5, we discuss the result of the numerical experiments. Finally, in section 6, we summarize this paper.

2. Spin-kicked rotor

As the target of numerical experiments, here we employ the spin-kicked rotor (the kicked rotor for a spin-$\frac{1}{2}$ particle (Scharf 1989)), which is composed of a two-level system and a rotor with instantaneous interactions ('kicks') at unit time intervals. We will use q and p to denote the position and the momentum of the rotor respectively and impose the periodic boundary condition with period 2π on q, $0 \leqslant q < 2\pi$. Then, the Hamiltonian of the spin-kicked rotor is the following:

$$\hat{H}(t) = T(\hat{p}) \otimes \hat{1}_{\mathrm{TLS}} + \sum_{n\in\mathbb{Z}} \delta(t-n)\hat{V}(\hat{q}) \tag{1}$$

where $T(p) = \frac{1}{2}p^2$ is the kinetic term of the rotor, $\hat{1}_{\mathrm{TLS}}$ is the identity operator of the two-level system and $\hat{V}(\hat{q})$ is the potential term acting on the total system. With c-number q, $\hat{V}(q)$ is an operator of the two-level system; accordingly, it can be decomposed as follows:

$$\hat{V}(q) = \phi(q)\hat{1}_{\mathrm{TLS}} + \boldsymbol{B}(q)\cdot\hat{\boldsymbol{\sigma}} \tag{2}$$

where $\boldsymbol{B}(q) = (B_x(q), B_y(q), B_z(q))$. The first term $\phi(q)\hat{1}_{\mathrm{TLS}}$ is the potential term which only affects the rotor for each kick, and the second term $\boldsymbol{B}(q)\cdot\hat{\boldsymbol{\sigma}}$ is the interaction term between the two-level system and the rotor. Since this model is a periodically driven quantum system, we introduce the Floquet operator $\hat{U}$ which governs a unit time evolution:

$$\hat{U} = \underset{\leftarrow}{\exp}\left\{\frac{1}{\mathrm{i}\hbar}\int_{n-0}^{n+1-0} \mathrm{d}t\ \hat{H}(t)\right\} \tag{3}$$

where $\underset{\leftarrow}{\exp}$ means the time ordered exponential and n is an arbitrary integer. Note that $\hat{U}$ does not depend on n, which means $\hat{U}$ represents stationary properties of this model. Using (1), $\hat{U}$ can be decomposed into the product of free part propagator $\hat{U}_{\mathrm{F}} = \exp\{\frac{1}{\mathrm{i}\hbar}T(\hat{p})\}\otimes\hat{1}_{\mathrm{TLS}}$ and the kick part propagator $\hat{U}_{\mathrm{K}} = \exp\{\frac{1}{\mathrm{i}\hbar}\hat{V}(\hat{p})\}$:

$$\hat{U} = \hat{U}_{\mathrm{F}}\hat{U}_{\mathrm{K}}. \tag{4}$$

In this paper, we choose $\phi(q) = K\cos q$ and $\boldsymbol{B}(q) = \delta K(\tilde{J}, 0, \cos q)$. As we shall see below, this is a case in which the spin-kicked rotor can be regarded as an extended version of the standard mapping describing by the Hamiltonian $\hat{H}_K(t) = \frac{1}{2}\hat{p}^2 + \sum_{n\in\mathbb{Z}}\delta(t-n)K\cos\hat{q}$ (Chirikov 1979, Casati *et al* 1979).

In order to investigate the qualitative nature of the dynamics, e.g. regular or chaotic, for a quantum system, we need a classical counterpart of the quantum system as we mentioned

earlier. Namely, if we find chaos in a classical system, the corresponding quantum system inherits the 'chaotic' nature from the classical system (Gutzwiller 1990). Although the spin-kicked rotor does not have the classical correspondent, in a naive sense, since the Hilbert space of the two-level system has the dimension 2 by definition, which may be too small to achieve the quantum-classical correspondence, we will seek 'classical counterparts' of the rotor subsystem in this paper. Here we employ a simple way to obtain a trajectory picture of the rotor. Since we will study only the weak 'tunnelling' case $\tilde{J} \ll 1$ in this paper, the Hamiltonian can be decomposed into three parts: two standard mappings described by the Hamiltonians for two manifolds $\sigma_z = \pm 1$, $\langle \uparrow |\hat{H}(t)| \uparrow \rangle = \hat{H}_{K+\delta K}(t)$ and $\langle \downarrow |\hat{H}(t)| \downarrow \rangle = \hat{H}_{K-\delta K}(t)$ and the tunnelling matrix element $J = \tilde{J}\delta K$ which causes tunnelling between the two manifolds during kicks in the two-level system. We can expect that the dynamics of the system can be regarded as just the superposition of two independent motions of two standard mappings in the first approximation, though this picture will break in the chaotic case as we shall see below. These two standard mappings have classical counterparts. Thus we can study the effects of the qualitative nature of the corresponding classical dynamics on the quantum system. We concentrate on the rather simple case $\delta K \ll K$, namely two standard mappings are almost the same and thus we can regard the single parameter K in this system as the nonlinear parameter, which controls the nature of the dynamics, regular or chaotic.

3. Polarization as a measure of quantum correlation

In our numerical experiments, we will measure the quantum mechanical correlation, namely, the degree of entanglement, between the two-level system and the rotor. For this purpose, here we introduce the polarization $P = |\langle \hat{\boldsymbol{\sigma}} \rangle|$ (Landau and Lifshitz 1977, section 59), which is the magnitude of the Bloch vector $\langle \hat{\boldsymbol{\sigma}} \rangle$ (Feynman *et al* 1957), where $\langle \cdot \rangle$ means the quantum mechanical average with the state that we supposed. Since we are interested in the quantum mechanical correlation between the subsystems, the two-level system and the rotor, we restrict ourselves to considering only pure states, which can be represented by state vectors without using the density matrix, as the states on which the above average $\langle \cdot \rangle$ and consequently the polarization P are evaluated. For the sake of the reader who is not familiar with describing the quantum correlation in the two-level system in terms of the polarization P (Landau and Lifshitz 1977, section 59), we here explain briefly the relationship between the polarization P and the reduced density matrix $\hat{\rho}$ of the two-level system. As is usual, the reduced density matrix $\hat{\rho}$ satisfies the inequality $0 \leqslant \mathrm{Tr}\,\hat{\rho}^2 \leqslant \mathrm{Tr}\,\hat{\rho} = 1$, supposing that $\hat{\rho}$ is normalized. The middle equality holds only when the two-level system is in a pure state and $\mathrm{Tr}\,\hat{\rho}^2$ becomes smaller when the two-level system is in a stronger mixed state, namely, it has stronger quantum correlation with the rotor. Accordingly, we can measure the degree of the quantum correlation between the two-level system and the rotor by the quantity $1 - \mathrm{Tr}\,\hat{\rho}^2$, which is equal to $\frac{1}{2} - \mathrm{Tr}\{(\hat{\rho} - \frac{1}{2})^2\} = \frac{1}{2} - \mathrm{Tr}\{\frac{1}{4}P^2\hat{1}_{\mathrm{TLS}}\} = \frac{1}{2}(1 - P^2)$, where we used the special property of the two-level system to derive the second expression from the first. Since $0 \leqslant P \leqslant 1$, we now know that larger (smaller) P means smaller (larger) quantum correlation between the two-level system and the rotor.

4. Numerical experiments and their interpretation

In order to elucidate effects of qualitative nature (e.g. regular or chaotic) of the rotor's dynamics (which has a classical counterpart) on the quantum correlation between the rotor

and the two-level system in the spin-kicked rotor, we will examine quantum-mechanical stationary states of the spin-kicked rotor for various values of the nonlinear parameter K by fixing other parameters. By examining stationary states of the system rather than its time evolution processes, we can reveal structures of the system (e.g. tunnelling doublets) more easily and clearly. The stationary states of the spin-kicked rotor model are eigenstates of the Floquet operator $\hat{U}$. We regard these eigenstates $\{|\phi_i\rangle\}_i$ of the Floquet operator $\hat{U}$ as to consist of an 'ensemble'; and define $\bar{P}$ as an 'ensemble average' of P_i with equal weight, where P_i is the polarization of the ith eigenstate $|\phi_i\rangle$.

At first, before we proceed to quantum mechanical results, we show how the classical dynamics of the rotor is changed when the parameter K is varied. Figure 1 shows Poincaré sections of two classical mappings generated from the Hamiltonians $\langle\uparrow\ |H(t)|\ \uparrow\rangle = H_{K+\delta K}(t)$ and $\langle\downarrow\ |H(t)|\ \downarrow\rangle = H_{K-\delta K}(t)$ for the up and the down manifolds, where $\delta K = 0.0625$. Since $\delta K \ll K \sim 1$, two Poincaré sections for each value of K ((*a*), (*b*) or (*c*)) are essentially the same in the global scale. As K increases, resonances grow (figure 1(*b*)) and finally global chaos emerges when K exceeds the critical value $K_c \sim 0.97$ (figure 1(*c*)) (Lichtenberg and Lieberman 1992, ch 4).

Figure 2 shows responses of the ensemble averaged polarization $\bar{P}$ to the variation of the nonlinear parameter K for three values of the Planck's constant h†. When h is very large (curve 1), the polarization $\bar{P}$ has a very weak dependence on the nonlinear parameter K and this almost constant value of $\bar{P}$ is very close to the possible maximum value 1. These two observations can be explained by remembering that large Planck's constant softens the detailed phase-space structure of the rotor's dynamics. Namely, large Planck's constant wipes out the difference of the dynamics of the rotor on the two manifolds, hence tunnelling becomes almost coherent and the polarization for these tunnelling states is almost 1. On the other hand, since the difference of the rotor's classical dynamics, i.e. regular or chaotic, is also softened, the nature of quantum dynamics of the spin-kicked rotor can exhibit only small differences. As Planck's constant h becomes smaller (curve 2, 3), the polarization $\bar{P}$ depends more strongly on the nonlinear parameter K. When h is small, $\bar{P}$ takes small values for $K \lesssim 0.5$ or $1.0 \lesssim K$, while it takes large values in the middle range $0.5 \lesssim K \lesssim 1.0$. In order to elucidate this non-monotonic dependency of $\bar{P}$ on K, next we study details of

† Here we explain the procedure that we employed to obtain numerically the eigenstates of the system. In order to achieve effectively the open boundary condition along the momentum space, we only consider the set of eigenstates that are selected by the following procedure. Such a procedure for selection is possible since all eigenstates in this quantum system are localized even though the corresponding classical system exhibits unlimited diffusion in time along the momentum axis (Casati *et al* 1979, Fishman *et al* 1982, Scharf 1989). First, by truncating the Hilbert space of the quantized rotor into the finite- (say, N-) dimensional Hilbert space, we impose the periodic boundary condition on the momentum space $-W_p/2 \leqslant p < W_p/2$, where $W_p = \hbar N$. Next, we numerically diagonalize the Floquet matrix of the truncated Hilbert space. We consider only the eigenstates that localizes within the momentum space $-W_p^{\rm cut}/2 \leqslant p < W_p^{\rm cut}/2$, where $W_p^{\rm cut}$ is small enough compared to W_p. Namely, the probability that the momentum is in the range $-W_p^{\rm cut}/2 \leqslant p < W_p^{\rm cut}/2$ for an eigenstate under consideration must be larger than the threshold. Hence, the boundary condition along the momentum axis actually does not have any influence on the eigenstates under consideration.

We employ $N = 128$ for $h/(2\pi)^2 = 0.038\,16$, $N = 256$ for $h/(2\pi)^2 = 0.015\,63$, and $N = 512$ for $h/(2\pi)^2 = 0.007\,816$. They correspond to the condition that $W_p \sim 8\pi$. As an exception, we employ $N = 1024$ for $h/(2\pi)^2 = 0.007\,816$ and $K = 2.0$ (this correspond to $W_p \sim 16\pi$). Since in this case the localization length $W_p^{\rm loc}$ in the momentum space has a large value $\sim 4\pi$ (in comparison, from the estimation with the diffusion constant for the classical system, $W_p^{\rm loc}/(2\pi) = 0.97$ (Shepelyansky 1986)) and we consequently need a larger value $\sim 16\pi$ for W_p. Since the difference of the numerical results with $N = 512$ and $N = 1024$ is small, we conclude that the values of N are large enough for precise diagonalizations. Especially, in calculating ensemble averaged polarizations, the difference between $N = 512$ and $N = 1024$ are less than 3% ($K = 2.0$, $h/(2\pi)^2 = 0.007\,816$). Thus we employ $N = 512$ for $h/(2\pi)^2 = 0.007\,816$ to draw figure 2, the nonlinear parameter dependence of the ensemble averaged polarization.

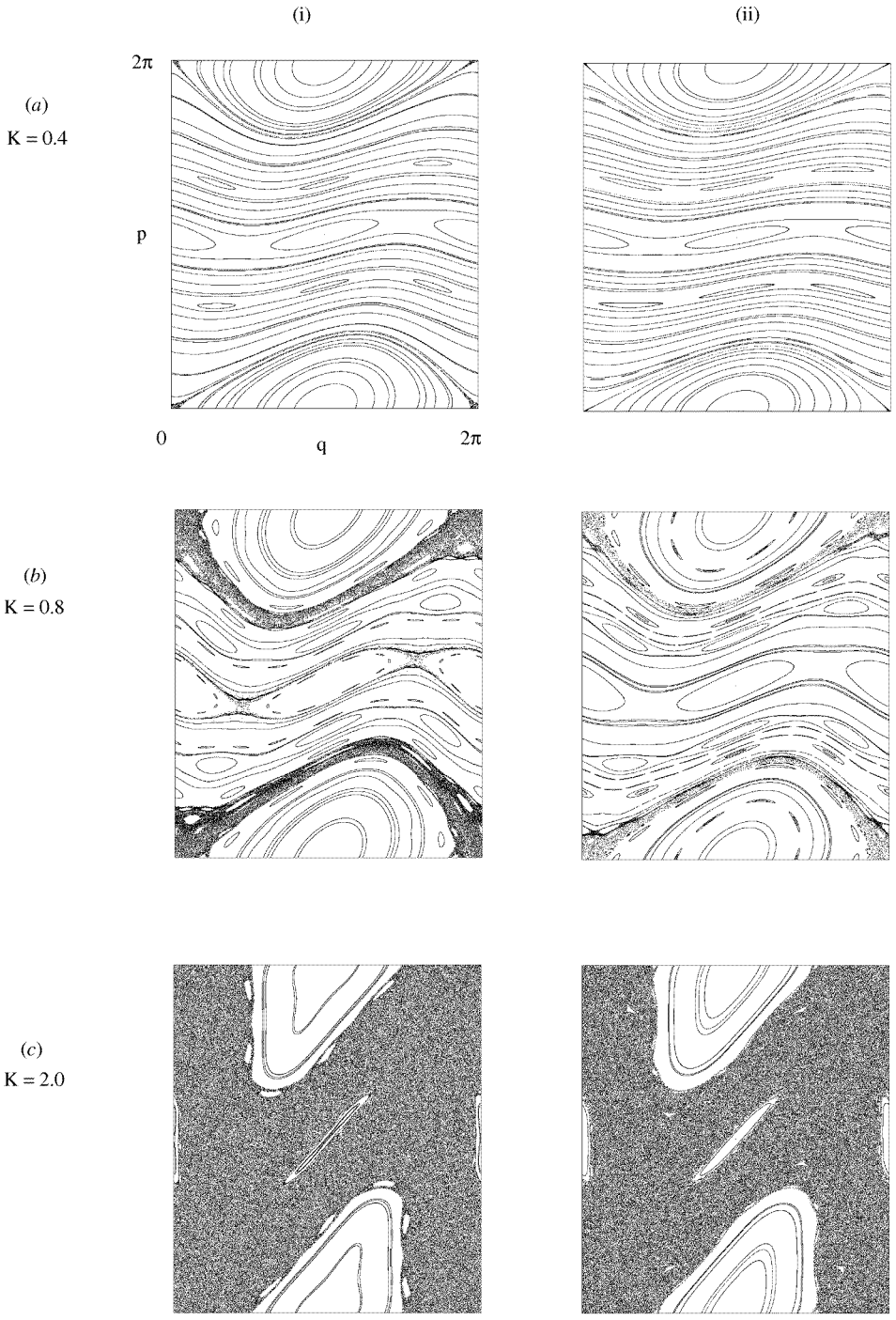

Figure 1. Poincaré sections of two classical mappings described by the Hamiltonians (i) $\langle\uparrow |\hat{H}(t)| \uparrow\rangle$ and (ii) $\langle\downarrow |\hat{H}(t)| \downarrow\rangle$ with the difference $\delta K = 0.0625$. The values of the nonlinear parameter K are (*a*) $K = 0.4$, (*b*) $K = 0.8$, and (*c*) $K = 2.0$.

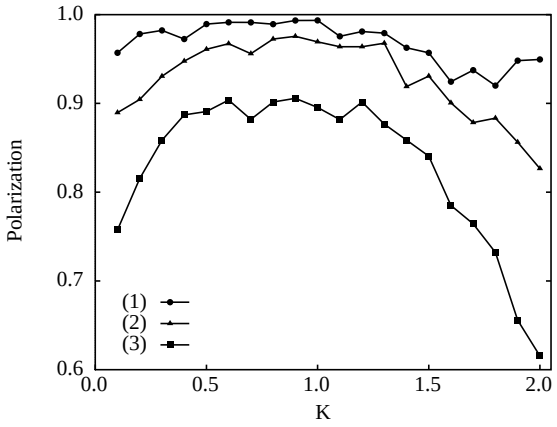

Figure 2. Responses of ensemble averaged polarization $\bar{P}$ to the nonlinear parameter K for three values of Planck's constant h (1) $h/(2\pi)^2 = 0.031\,26$, (2) $h/(2\pi)^2 = 0.015\,63$, and (3) $h/(2\pi)^2 = 0.007\,816$. Other parameters in the numerical experiments are $\delta K = 0.0625$ and $\tilde{J} = 0.0625$.

ensembles in the case $h/(2\pi)^2 = 0.007\,328$, which corresponds to the curve 3 in figure 2.

Figure 3(i) depicts the correlation between the expectation value of rotor's momentum p and the polarization P in the ensemble of eigenstates. Since the phase-space dynamics of the rotor has the translation symmetry $(q, p) \to (q, p + 2\pi)$ along the momentum axis and the parity symmetry $(q, p) \to (-q, -p)$, the momentum expectation value of each eigenstate is reduced into the range $0 \leqslant p \leqslant \pi$ according to these symmetries in the figure. In order to explain the accumulation of points in figure 3(i), the distributions of polarizations are depicted in figure 3(ii).

4.1. $K = 0.4$: regular dynamics, vivid tunnelling

First, let us consider figure 3(*a*), for which $K = 0.4$ and the corresponding classical dynamics is very regular. In this case, we can interpret the graph very easily by remembering the rotor's phase space structure of the corresponding classical dynamics (figure 1(*a*)). The points accumulated on a vertical line at $p = 0$ correspond to the libration around the fixed points $(q, p) = (\pi, 2\pi n)$ for $n \in \mathbb{Z}$. These accumulated points are gathered from the range $0 \leqslant p \lesssim \pi/3$ due to the locking mechanism in the libration. Most of these points have a large polarization P close to 1, though some of them have small values (≈ 0.5). A similar structure is observed at $p = \pi$. On this occasion, the locking comes from the librational motion around the period-2 periodic points $(q, p) = (0, (2n + 1)\pi), (\pi, (2n + 1)\pi)$ for $n \in \mathbb{Z}$. On the other hand, the other points in the range $\pi/3 \lesssim p \lesssim \pi$ lie on a one-dimensional smooth curve. This one-to-one smooth functional relationship between p and P in quantum mechanics is a result of the regular phase space structure of the corresponding classical dynamics (Toda and Ikeda 1987). These points on the curve corresponds to the rotation. Though the points have relatively large values of P, which are close to 1, we observe that this curve has a concave hollow around $p = 3\pi/4$, where the polarization P takes ≈ 0.8. This hollow is the origin which reduces the ensemble averaged polarization $\bar{P}$ due to the large number of states belonging to the hollow, when K is small (curve 3 in figure 2). In fact, most (80–90%) of these eigenstates whose polarization is reduced from 1

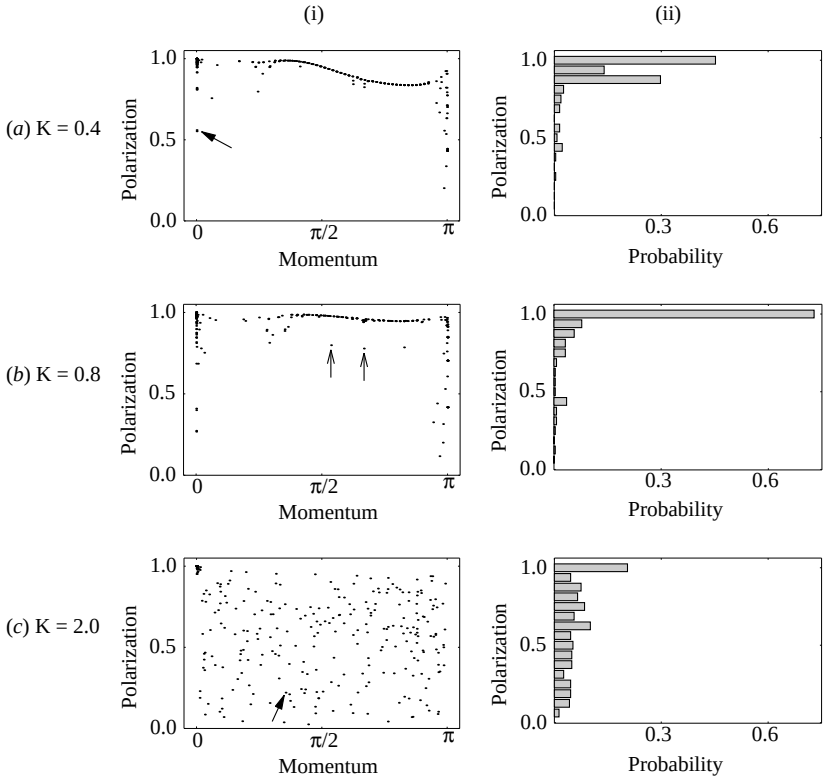

Figure 3. (i) Correlations between the expectation value of the momentum of the rotor p and the polarization P for stationary states in the case $h/(2\pi)^2 = 0.007\,816$, where one point corresponds to one eigenstate. The values of the nonlinear parameter K are (*a*) $K = 0.4$, (*b*) $K = 0.8$, and (*c*) $K = 2.0$. Other parameters are the same as in figure 2. Arrows in (*a*) and (*c*) indicate states which are shown in figures 4 and 6. Two states arrowed in (*b*) will be explained in the main text. (ii) Distributions of the values of the polarization.

to ≈ 0.5–0.8 form pairs of 'tunnelling doublets', which was explained before. In figure 4, we visualize the Hushimi distribution function for a pair of such tunnelling doublets, which are pointed by an arrow in figure 3(*a*). These eigenstates have small polarizations in the graph. The reason why these eigenstates have such low polarizations and extend to both of the up and the down manifolds ($\sigma_z = +1$ and -1) of wavefunctions can be understood as follows. If the tunnelling matrix element J does not exist, each eigenstate should localize in either the up or the down manifold. When we turn on J as a perturbation, two unperturbed eigenstates whose eigenangles are almost degenerate are accidentally mixed up by the perturbation to form a pair of tunnelling doublets. We can calculate the degree of mixture, namely, the decrease of the polarization by perturbation theory; we will derive the perturbed polarization P in appendix A:

$$P = \left(\frac{1 + 4|S|^2 (|J_{\mathrm{eff}}|/\Delta E^{\mathrm{unpert}})^2}{1 + 4(|J_{\mathrm{eff}}|/\Delta E^{\mathrm{unpert}})^2} \right)^{\frac{1}{2}} \tag{5}$$

where $\Delta E^{\mathrm{unpert}}$ and S are the difference of energies and the overlapping integral for two unperturbed states respectively and the quantity J_{eff} is the effective tunnelling matrix element

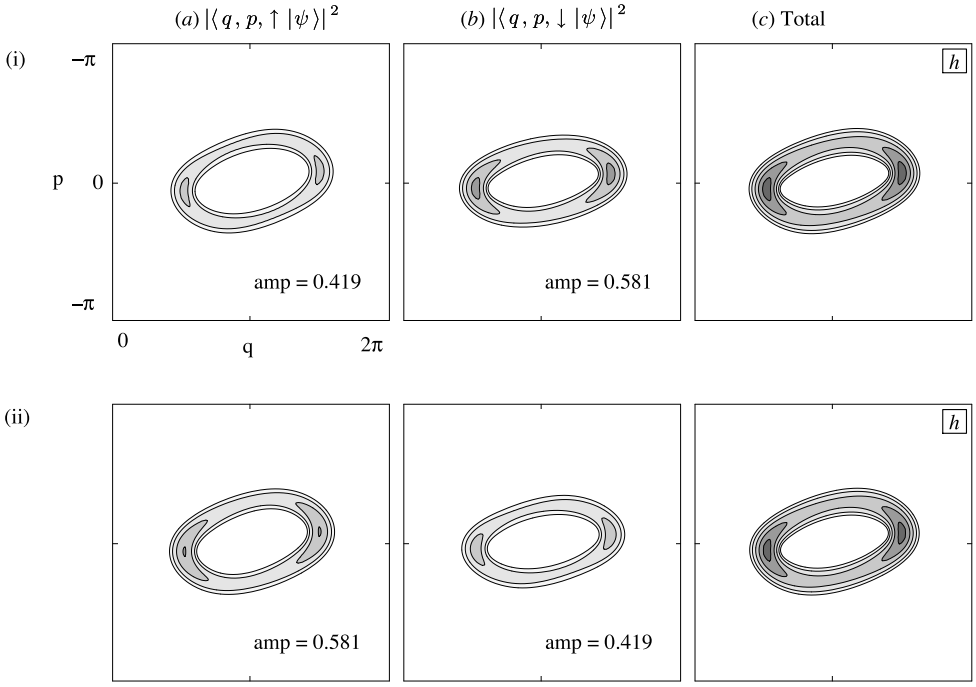

Figure 4. Hushimi distribution functions of a pair of tunnelling doublets ($K = 0.4$, $h/(2\pi)^2 = 0.007\,816$) (i) 'symmetrical' state $\psi_{\rm s}$ and (ii) 'asymmetrical' state $\psi_{\rm a}$. These tunnelling doublets are composed of two localized states which are the 15th state on the up manifold and the 13th state on the down manifold. Quasienergies (mod $h = 0.308\,58$) of ψ_s and ψ_a are 1.97×10^{-3} and 2.39×10^{-3}, respectively. Three Hushimi functions (*a*) $|\langle q, p, \uparrow |\psi\rangle|^2$, (*b*) $|\langle q, p, \downarrow |\psi\rangle|^2$ and (*c*) their summation are drawn for each eigenstate ψ, where the amplitude of each component is shown in the plots. Polarization of the states ψ_s and ψ_a are 0.560 and 0.552, respectively. The area corresponding to Planck's constant h is indicated by a square.

and is defined in (A11). In appendix A, we also obtain an approximate relationship

$$J_{\rm eff} \simeq J S. \tag{6}$$

In our explanation of the entangled states with the tunnelling doublets picture, the polarization P, our measure of entanglement is governed by two parameters according to (5) and (6). One is $\Delta E^{\rm unpert}$, which is the distance in energy between two unperturbed states; the smaller $\Delta E^{\rm unpert}$ becomes, the easier it becomes to mix two unperturbed states that are localized on the up and the down manifolds, respectively. Things are the same for ordinary tunnelling processes. The other parameter is $|S|$, the magnitude of the overlapping between the rotor's components of the unperturbed states. It has two meanings. On the one hand, $|S|$ determines the magnitude of $J_{\rm eff}$ through (6). Especially, $|S| \to 0$ means $J_{\rm eff} \to 0$. Consequently, two unperturbed states do not mix through the perturbation and $P \to 1$. On the other hand, $|S|$ determines the degree of coherence of the tunnelling doublets. For example, when $|S| \to 1$, the tunnelling doublets become coherent. Hence the polarization P becomes unity. Assume that the state of the system is described by the Hilbert space spanned by a pair of tunnelling doublets. Then, when $|S|$ becomes smaller, it becomes easier to guess on which manifold, up or down, the two-level system is found after the rotor part of the system is observed. Namely, with fixed value of $|J^{\rm eff}|/\Delta E^{\rm unpert}$, the quantum mechanical correlation (entanglement) between the rotor and the two-level system

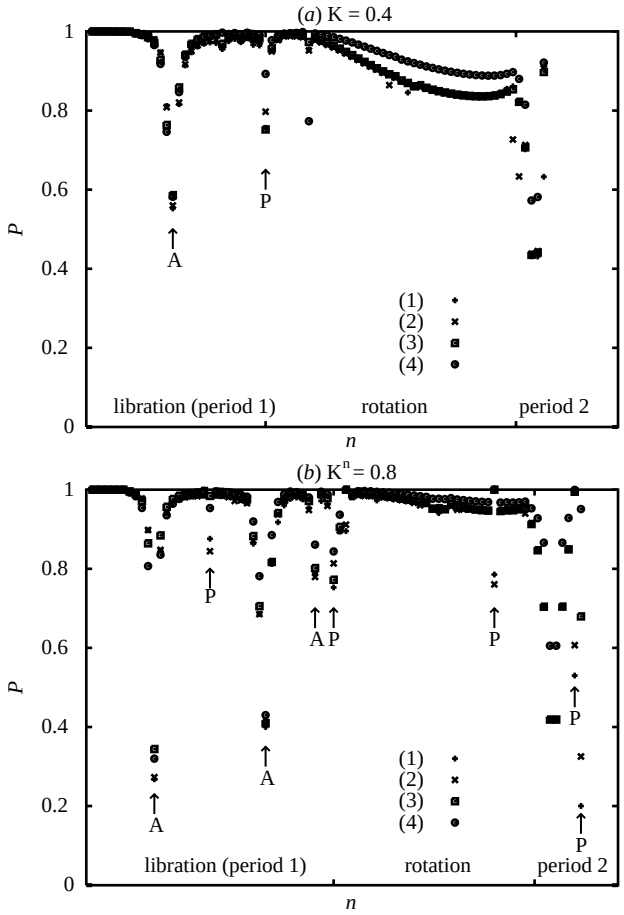

Figure 5. Quantum number of a pair of tunnelling doublets n versus polarization P. As is explained in the main text, there are four values of P for single value of n: (1) polarization of one doublet that has larger probability on the up manifold; (2) polarization of the other doublet that has larger probability on the down manifold; (3) perturbation theory (5); (4) perturbation theory (5), with the approximation (6) for $J_{\rm eff}$. The values of the nonlinear parameter K are (*a*) $K = 0.4$, (*b*) $K = 0.8$. Other parameters are $h/(2\pi)^2 = 0.007\,816$, $\delta K = 0.0625$ and $\tilde{J} = 0.0625$.

becomes stronger (i.e. P becomes smaller) when $|S|$ becomes smaller. This is the particular situation for the entanglements; there is no corresponding phenomenon for tunnellings.

In figure 5, we compared with the perturbation theory (5) and the numerical experiments in the regular region ($K = 0.4, 0.8$), by plotting the values of polarization. We represent, in the figures, the eigenstates that can be regarded as tunnelling doublets and have supports in the momentum space $0 < p < \pi$. Since the systems are regular, we can assign quantum numbers for the eigenstates. In the figures, we employ the quantum number for the horizontal axis. First, we explain the assignment of quantum numbers in the following. We assign a quantum number $n = 0$ to the 'ground state' among the librational eigenfunctions that are centred at $(q, p) = (\pi, 0)$. We regard the rotational eigenstates as the 'excited' states to the librational states. Accordingly, we assign higher quantum numbers to the rotational eigenstates. Next, we plot the values of polarization corresponding to

the tunnelling doublets; from the numerical experiment, a pair of doublets has two values of polarization for each doublet; from the perturbation theory (5), we have one value of polarization for a pair of doublets. At the same time, we show the values of the perturbed polarization (5) by employing the approximation (6) for the tunnelling matrix element $J_{\rm eff}$. For these values, we found systematic errors in the rotational region compared to the case without the approximation (6). This is because the approximation (6) has 20–40% relative errors.

As we can see in figure 5, for most of entangled states, the perturbation theory (5) explains the numerical experiments well. In the figure, we point out several valleys with arrows marked 'A'. They correspond to the tunnelling doublets that have small polarization due to the accidental near-degeneracies. (In fact, the tunnelling doublets that we show in figure 4 correspond to the valley shown in figure 5(a).)

Next, we explain the case in which the perturbation theory (5) does not work well. In figure 5, we point out cave-ins with arrows marked 'P'. These entangled states are, in fact, not tunnelling doublets and have significant contributions from more than two unperturbed states. In addition, some eigenstates (10–20%) cannot be regarded as doublets. Namely, in order to apply a perturbation theory for J on these entangled states, we must incorporate more than two (3–8) unperturbed states. Here we explain by an example that these entangled states emerge due to the regular structure of the unperturbed system. Let us consider two entangled states that are pointed by arrows in figure 3(b) and are placed out of the smooth curve along $\pi/2 < p < \pi$ in the figure. The entangled states are mainly composed of two unperturbed states that correspond to the period-4 and the period-3 rotations of the rotor on the up and the down manifolds, respectively. These two unperturbed states are nearly degenerate but have only small overlap. Consequently, the perturbation formula (5) gives a poor estimation $P = 1.0$. We point out the reason for the breakdown of the perturbation formula for these entangled states by elucidating their structure. This is due to the contribution to the entangled states from the unperturbed state that correspond to the period 3 rotational motion of the rotor on the up manifold. It has a large overlap with the state corresponding to the period-3 rotational motion on the down manifold, despite of the large energy spacing between them. Accordingly, it becomes important to incorporate the 'third' state in addition to the two nearly-degenerate states for these entangled states†. Hence, we obtained the entangled states that are not tunnelling doublets due to the (pre-overlapping) resonance. As we can see in the scatter of points among $0 < p < \pi/3$ in figure 3(i), these effects make the locking structure due to the classical libration imperfect.

4.2. $K = 0.8$: regular dynamics, suppressed tunnelling

When K is increased from 0.4 (figure 3(a)) to 0.8 (figure 3(b)), keeping the classical dynamics to be regular, we notice that, in these figures, the one-dimensional branch around $2\pi/3 \lesssim p \lesssim \pi$ corresponding to the rotational motion moves upward. Consequently, in figure 2, the averaged polarization $\bar{P}$ becomes larger when K is increased in the regular region $0 \leqslant K \lesssim K_{\rm c} \sim 1$. In this paragraph, we will explain why the polarization of the eigenstates on the rotational branch becomes larger, when K is increased in the regular

† Bohigas, Tomsovic and Ullmo found that the parameter dependences of the energy splitting for tunnelling doublets behave irregularly under the influence of the 'chaotic states', to which a quantum number cannot be assigned through the EBK semiclassical quantization procedure (Einstein 1917, Brillouin 1926, Keller 1958). In contrast to this, our result suggests that the 'regular' states can complicate the parameter dependence for the energy splitting of the tunnelling doublets. However, this is a pseudo-complication, since it can be explained in terms of the regular structure of the unperturbed system as is explained in the main text.

region, based upon formulae (5) and (6) from the perturbation theory. Formulae (5) and (6) have two parameters S and ΔE^{unpert} which concern the unperturbed system, where S is the overlapping between two unperturbed states and ΔE^{unpert} is the energy difference of the two unperturbed states. In our case, the two unperturbed eigenstates are the rotational eigenstates of the two quantum standard mappings corresponding to the separated up and down manifolds, for which the values of the nonlinear parameter K are $K + \delta K$ and $K - \delta K$, respectively. Furthermore, the two rotational eigenstates have the same value for the quantum number n of the quantum standard mapping in the regular region. Accordingly, we will express these unperturbed eigenstates as $|\phi_n(K + \delta K)\rangle$ and $|\phi_n(K - \delta K)\rangle$, where $|\phi_n(K)\rangle$ is the nth rotational eigenstate of the quantum standard mapping with the nonlinear parameter K.

By using these states, the energy difference ΔE^{unpert} and the overlapping S, which determine the polarization P through (5) and (6), are calculated as

$$\Delta E^{\text{unpert}} \equiv E_n(K + \delta K) - E_n(K - \delta K) \tag{7}$$

$$S \equiv \langle \phi_n(K + \delta K) | \phi_n(K - \delta K) \rangle \tag{8}$$

where $E_n(K)$ is the nth rotational eigenenergy of the quantum standard mapping with the nonlinear parameter K.

As we mentioned earlier, the perturbed polarization formula (5) explains the numerical result well. Furthermore, in appendix B, concerning to the two inputs ΔE^{unpert} and $|S|$ to the formula, we observe that the values of ΔE^{unpert} become twice as large and the values of $|S|$ stay constant when we increase the nonlinear parameter K from 0.4 to 0.8. By substituting these results in appendix B to formulae (5) and (6), these formulae explain the increase of the polarization for rotational states observed from figure 3(a) to figure 3(b), which was mentioned before.

Consequently, we can say that since the difference of the two unperturbed eigenenergies in a pair of doublets ΔE^{unpert} becomes larger, keeping the same order of magnitude of $|S|$, the tunnelling between the two manifolds becomes more difficult and the polarization for the pair P becomes larger when K is increased from 0.4 to 0.8. Accordingly, the hollow in figure 3(a) disappears in figure 3(b) and the averaged polarization $\bar{P}$ takes lager value in the latter case.

Furthermore, in appendix B, the above parameter dependences of ΔE and S upon K, $\Delta E \sim CK$ with $C > 0$ and $S \sim$ constant, will be explained by a simple semiclassical analysis for a pendulum.

4.3. $K = 2.0$: chaotic dynamics, chaotic entangled state

When K is increased further, global stochasticity emerges in the corresponding classical systems. Although the transition to global stochasticity is softened by non-zero Planck's constant in the quantum system as usual, the quantum correlations, i.e. the quantum entanglements, begin to be created at $K \sim K_c$ due to the stochasticity. Figure 3(c) shows the disappearance of the structure in the correlation between the expectation value of the rotor's momentum p and the polarization P. This is due to the quantum correspondent of the resonance overlapping (Toda and Ikeda 1987). Most of the eigenstates are entangled except around the rotor's elliptic points $(q, p) = (\pi, 2\pi n)$ for $n \in \mathbb{Z}$ where the dynamics of the rotor still remain regular. These entangled states cannot be localized on a manifold. Accordingly, the polarization P for these eigenstates extended on both manifolds can take any value from the range $0 \leqslant P \leqslant 1$ depending on the degree of the extendedness. Many eigenstates have complicated patterns in phase space, when visualized by the Hushimi

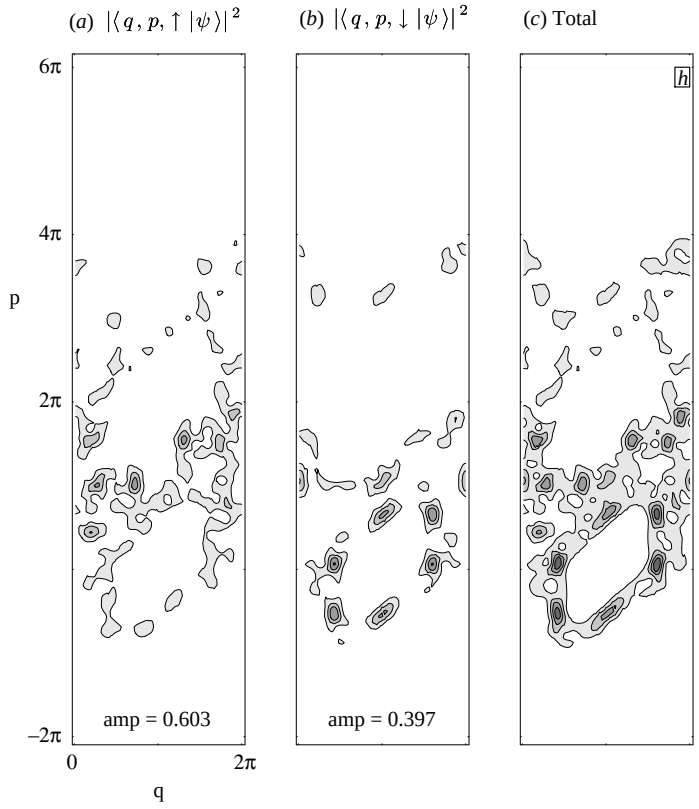

Figure 6. Hushimi functions of a chaotic entangled state ($K = 2.0$, $h/(2\pi)^2 = 0.007\,816$). Three plots are shown in the same way as in figure 4. The polarization of the state is 0.188. The area corresponding to Planck's constant h is indicated by a square.

function (Hushimi 1940, Takahashi and Saitô 1985) (see figure 6) and are clearly different from ones in the regular stage. These chaotic entangled states are different from tunnelling doublets (the regular entangled states) in the regular region. Both entangled states are more or less extended on both manifolds by definition. However, for almost all regular entangled states (80–90%), each state has the twin brother; the twins forms tunnelling doublets (see figure 4). On the other hand, any chaotic entangled states never have a twin brother. A chaotic entangled state is shown in figure 6.

We explain how the chaotic entangled states are described by the perturbation theory on the tunnelling matrix element J. Especially, we emphasize the difference to the case for the regular entangled states. First of all, we introduce the entropy of an eigenstate $|\psi\rangle$ defined by the eigenstates of the unperturbed system:

$$\mathcal{H}(|\psi\rangle) = -\sum_{n}\sum_{\sigma=\uparrow,\downarrow} p_{n\sigma}\log p_{n\sigma} \tag{9}$$

where

$$p_{n\uparrow} = |\langle\phi_n(K+\delta K), \uparrow |\psi\rangle|^2 \tag{10}$$

$$p_{n\downarrow} = |\langle\phi_n(K-\delta K), \downarrow |\psi\rangle|^2. \tag{11}$$

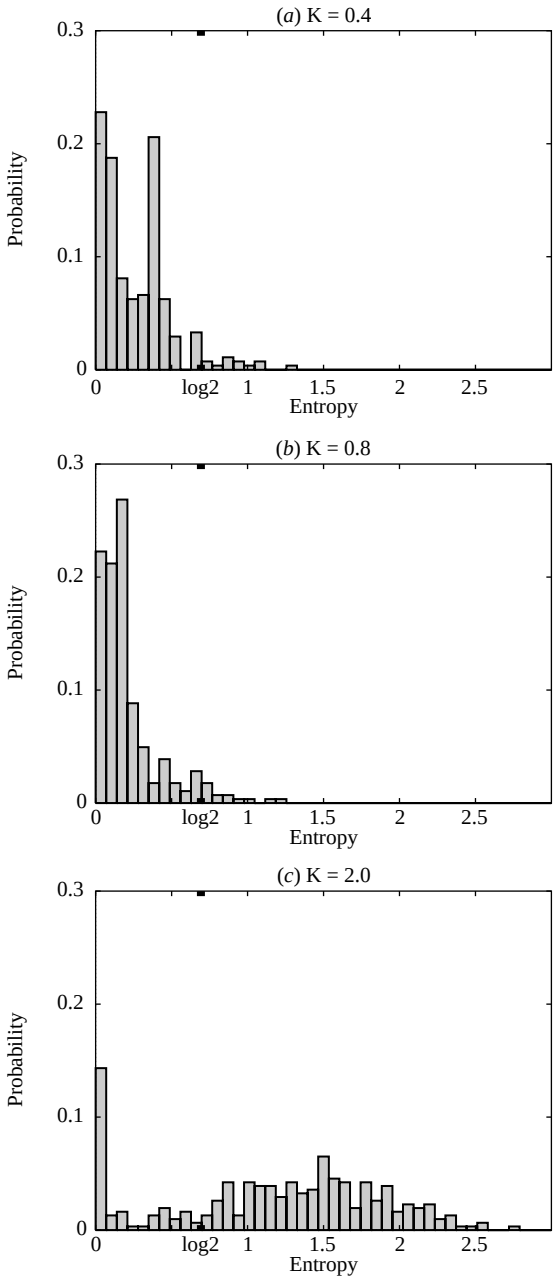

Figure 7. Distributions of the value of the entropy (9) of the stationary state. The value of the Planck constant is $h/(2\pi)^2 = 0.007\,816$. The values of the nonlinear parameter K are (a) $K = 0.4$, (b) $K = 0.8$, (c) $K = 2.0$. Other parameters are the same as in figure 2.

Two sets of eigenstates $\{|\phi_n(K+\delta K)\rangle\}_n$ and $\{|\phi_n(K-\delta K)\rangle\}_n$ are the sets of eigenstates of the standard mapping on the up and the down manifolds, respectively, for the unperturbed system. Hence, the entropy $\mathcal{H}(|\psi\rangle)$ represents the logarithm of how many unperturbed

states the state $|\psi\rangle$ is spanned by. We note that the entropy defined here essentially depends on the unperturbed states. In figure 7, we show the distributions of $\mathcal{H}(|\psi\rangle)$. We explain the figure as follows. In the distributions, the peak at $\mathcal{H} = 0$ corresponds to the eigenstates that are changed only little by the perturbation. In addition to this, in figure 7(a) ($K = 0.4$), we have a peak at $\mathcal{H} \sim 0.4$. This corresponds to the tunnelling doublets. By comparing the value of the entropy with $\log 2$, which represents the case in which a tunnelling doublet is composed of two unperturbed states with equal weight, it is clear that most tunnelling doublets are biased to one of the unperturbed states. This is because the values of the nonlinear parameters of two standard mappings in the unperturbed system are different. (In terms of the tunnellings in the double well potential, the asymmetry of the potential corresponds to the reason for the biases.) In figure 7(b) ($K = 0.8$), the peak that characterizes the existence of a tunnelling doublet at $K = 0.4$ disappears. At the same time, the peak at $\mathcal{H} = 0$ broadens. As we explained earlier, this is because the entanglements of the tunnelling doublets are destroyed due to the increase in the value of the nonlinear parameter K. In the figure for the chaotic rotor (figure 7(c), $K = 2.0$), there still remains the peak at $\mathcal{H} = 0$. This corresponds to the regular states around the elliptic fixed points at $(q, p) = (\pi, 2\pi n)$ ($n \in \mathbb{Z}$). In contrast to this, the broad (width ~ 1.2) peak at $\mathcal{H} \sim 1.6$ corresponds to the chaotic entangled states. A chaotic entangled state is spanned by approximately $\exp(\mathcal{H})$ unperturbed states (e.g. for the state corresponding to the peak of $\mathcal{H}$ is spanned by $\exp(1.6) = 4.95$ unperturbed states.) Hence, in order to obtain only one eigenstate by the perturbation theory for J, we must incorporate a set of many unperturbed states. Furthermore, differently to the regular region, since it becomes impossible to assign proper structure for the unperturbed states, we can characterize the set of unperturbed states only by the range of the (quasi-) energies. We explain the reason why we must incorporate so many states in order to execute the perturbation theory in the chaotic region. First, we remember the regular region. In this case, the entangled states are composed of the unperturbed states that are in the 'neighbourhood' in the phase-space representation (the Hushimi representation). Apart from this, we have near-degeneracies of the unperturbed states. However, even they are strongly near-degenerate, since they are far apart in the phase-space representation, they are not mixed by the weak perturbation to compose entangled states. When the system becomes chaotic, these states spread in the phase-space representation due to the resonance overlapping. Accordingly, they become easier to be mixed by the 'weak' (in this case, the same order of magnitude compared with the regular case mentioned above) perturbation to produce the chaotic entangled states, even though unperturbed eigenenergies repel. In other words, in the regular case, since the amplitude of unperturbed states in the phase space representation are concentrated in an area, they can produce entangled states thanks to the relatively large overlapping integral even if they are far apart in the eigenenergies. In contrast to this, in the chaotic case, even if the overlapping between two unperturbed states are relatively small, in the narrow range of the eigenenergy, there are many unperturbed states that are able to be mixed by the perturbation to produce the chaotic entangled states. The results of the numerical experiments support this explanation. On one hand, for a set of regular entangled states, the (quasi-) energy spacings $\Delta E^{\mathrm{split}}$ among them are $\Delta E^{\mathrm{split}}/h \sim 10^{-2}$, except for accidental near-degeneracies. On the other hand, for a set of chaotic entangled states, $\Delta E^{\mathrm{split}}/h \sim 10^{-3}$. Finally, in order to complete the whole procedure of the perturbation theory, we must diagonalize the Floquet matrix that is truncated into the Hilbert space that is spanned by the set of unperturbed states. As we often see, we cannot generally give the clear physical interpretation of the eigenstate only by diagonalizing the Floquet matrix or the Hamiltonian of the system. Hence, our perturbational analyses presented here do not give a clear physical picture for the chaotic

entangled states, though they could for the regular entangled state.

5. Discussion

We discuss two topics concerning our results of the numerical experiments. First, we explain the relationship between our result and the previous studies on the influences of chaotic dynamics on quantum mechanical tunnelling phenomena. Second, we summarize our result in terms of a semiclassical theory to give an outlook.

We studied in this paper the quantum mechanical entanglements between the two-level system and the rotor in the spin-kicked rotor. At the same time, it is interesting to discuss the relationship between our result and the influences of chaotic dynamics on quantum mechanical tunnelling phenomena. Before we explain this relationship, we refer to the previous works on the influences of chaos on tunnelling (Roncaglia *et al* 1994, Bohigas *et al* 1993, Tomsovic and Ullmo 1994, Utermann *et al* 1994). In particular, in the former three works, they studied the tunnelling doublets themselves. On the other hand, Utermann *et al* observed how the tunnelling doublets are destroyed under the influence of the chaotic diffusion in phase space. They find, for the tunnelling doublets, that the energy splitting and the overlapping of the Hushimi functions with the chaotic region in the phase space are strongly correlated. Hence, they concluded that by touching the chaotic region in the phase space, a pair of tunnelling doublets breaks up their tunnel splitting (Utermann *et al* 1994). However, from the viewpoint employed in the above four works, it is impossible to discuss the role of the well-developed chaotic dynamics for the tunnelling processes. Keeping this in mind, we discuss our result as a problem of quantum mechanical tunnellings. Since, in the spin-kicked rotor, we assign two subsystems, the two-level system and the rotor, to the coherent tunnelling and the chaotic diffusive degrees of freedom respectively, we can discuss the role of the well developed chaotic dynamics for the tunnelling processes. The followings are our conclusion for the influences of the rotor's dynamics on the incoherent tunnelling processes between the up and the down manifolds in the two-level system. When the dynamics of the rotor is regular and the value of the nonlinear parameter is small, many tunnelling doublets are produced due to the accidental near-degeneracies in the unperturbed system, which has a zero tunnelling matrix element. By changing the value of the nonlinear parameter in the regular region, the accidental near-degeneracies are generally destroyed. Accordingly, the tunnelling processes due to the doublets are suppressed. When the dynamics of the rotor is chaotic, the tunnelling processes in the two-level system are enhanced by the chaotic entangled states. Finally, we point out the most important difference between the tunnelling processes due to the tunnelling doublets and the chaotic entangled states. With the tunnelling doublets, the tunnelling process is simple since there is only one characteristic tunnelling frequency that is determined by the energy splitting of the doublet. One the other hand, the tunnelling processes due to the chaotic entangled states have many characteristic frequencies since the chaotic entangled states involve many unperturbed states that localize on a manifold in the two-level system (cf figure 7(*c*)). Thus such tunnelling processes are far more complex than ones in the regular region (cf Shudo and Ikeda 1995).

Next, we summarize our numerical experiments in terms of semiclassical theory in order to seek a more clear physical picture for the chaotic entangled states than in terms of perturbation theory, which was employed in section 4. When the dynamics of the corresponding classical rotors is regular, each entangled state is a 'tunnelling doublet'. Such a tunnelling doublet is composed of the two unperturbed states which are localized on the up ($\sigma_z = +1$) and the down ($\sigma_z = -1$) manifolds of the two-level system. These localized states on both manifolds can be understood quite well in terms of classical dynamics of

the kicked rotors described by the Hamiltonians $\hat{H}_{K+\delta K}$ and $\hat{H}_{K-\delta K}$. Since the classical dynamics described by the either Hamiltonian is regular, the well established theory of semiclassical quantization for regular systems, which is called the Einstein–Brillouin–Keller (EBK) quantization (Einstein 1917, Brillouin 1926, Keller 1958), can be applied to the split system on the upper or lower manifold. A resultant eigenfunction should be concentrated on some invariant torus, which is selected by the EBK rule. At the next step, in order to complete the semiclassical quantization of the whole system, it is enough to incorporate the weak tunnelling effect as a perturbation to the unperturbed systems split into the upper and the lower manifolds. On the other hand, in the chaotic stage ($K_c \ll K$), the 'tunnelling doublet' picture cannot be applied. The dynamics of the rotor and the two-level system cannot be separated as in the regular stage. Namely, from the beginning, we must incorporate the transition between the upper and the lower manifolds due to the tunnelling effect, which does not exist in the usual classical dynamics, with the rotor's dynamics, in order to perform some semiclassical quantization for the chaotic spin-kicked rotor. The procedure to perform the semiclassical quantization for such a chaotic system living on multiple potential surfaces has been desired for a long period. However, none has yet succeeded in inventing something that really works.

6. Summary

We summarize our work as follows. We studied the quantum mechanical entanglements of the spin-kicked rotor in weak coupling case between the two-level system and the rotor. As a measure of entanglement, we employed the polarization of the two-level system. In the numerical experiments, we found that the nature of quantum mechanical entanglements changes drastically according to the change of the nature of the corresponding classical dynamics from regular to chaotic in the semiclassical region. With the regular rotor, entangled states are generally tunnelling doublets. On the other hand, with the chaotic rotor, any entangled state has no twin brother and we named these states chaotic entangled states.

Acknowledgments

I am grateful to Dr S Adachi for helpful discussions and improving this manuscript and to Professor K Kitahara for encouragement and support. I wish to thank one of the anonymous referees of *J. Phys. A: Math. Gen.* for giving detailed comments and advice, which were essential for the improvement of the manuscript.

Appendix A. A derivation of the polarization (6) by a degenerate perturbation method

In this appendix, we derive a formula (5) for the polarization P of the eigenstate $|\Psi\rangle$ of the spin-kicked rotor with a perturbation method.

We start our derivation for a more general system described by the Floquet operator $\hat{U}$

$$\hat{U} = \exp\left\{\frac{1}{\mathrm{i}\hbar}\hat{T}\right\}\exp\left\{\frac{1}{\mathrm{i}\hbar}(\hat{V}_0 + \epsilon\hat{W})\right\} \tag{A1}$$

where $\epsilon\hat{W}$ is the perturbation for the unperturbed Floquet operator $\hat{U}_0$

$$\hat{U}_0 = \exp\left\{\frac{1}{\mathrm{i}\overline{h}}\hat{T}\right\}\exp\left\{\frac{1}{\mathrm{i}\overline{h}}\hat{V}_0\right\}. \tag{A2}$$

Without the perturbation $\epsilon\hat{W}$, eigenkets $|\phi\rangle$ and $|\psi\rangle$ of $\hat{U}_0$ have quasienergies f and g, respectively; i.e. $\hat{U}_0|\phi\rangle = |\phi\rangle \mathrm{e}^{f/\mathrm{i}\overline{h}}$ and $\hat{U}_0|\psi\rangle = |\psi\rangle \mathrm{e}^{g/\mathrm{i}\overline{h}}$. Assume that quasienergies f and g are nearly degenerate (i.e. $\Delta E^{\mathrm{unpert}}/\overline{h} = (f-g)/\overline{h} = \mathcal{O}(\epsilon)$), then a ket $|\Psi\rangle = |\phi\rangle\alpha + |\psi\rangle\beta$ is an approximate eigenstate of $\hat{U}$. In this case, the eigenvalue equation

$$\hat{U}|\Psi\rangle = |\Psi\rangle \mathrm{e}^{E/\mathrm{i}\overline{h}} \tag{A3}$$

becomes the following equation for a vector $(\alpha \quad \beta)$:

$$\hat{U}_{\mathrm{trunc}}\begin{pmatrix}\alpha\\ \beta\end{pmatrix} = \begin{pmatrix}\alpha\\ \beta\end{pmatrix}\mathrm{e}^{E/\mathrm{i}\overline{h}} \tag{A4}$$

where

$$\hat{U}_{\mathrm{trunc}} = \begin{pmatrix}\langle\phi|\hat{U}|\phi\rangle & \langle\phi|\hat{U}|\psi\rangle\\ \langle\psi|\hat{U}|\phi\rangle & \langle\psi|\hat{U}|\psi\rangle\end{pmatrix}. \tag{A5}$$

Next, we introduce a unitary operator

$$\hat{U}_{\mathrm{perturb}} = \exp\left(-\frac{1}{\mathrm{i}\overline{h}}\hat{V}_0\right)\exp\left\{\frac{1}{\mathrm{i}\overline{h}}(\hat{V}_0 + \epsilon\hat{W})\right\} \tag{A6}$$

so that the equation $\hat{U} = \hat{U}_0 \cdot \hat{U}_{\mathrm{perturb}}$ holds. This unitary operator $\hat{U}_{\mathrm{perturb}}$ can be expressed as

$$\hat{U}_{\mathrm{perturb}} = \underset{\leftarrow}{\exp}\left\{\frac{\epsilon}{\mathrm{i}\overline{h}}\int_0^1 \mathrm{d}\tau\ \hat{W}(\tau)\right\} \tag{A7}$$

where $\underset{\leftarrow}{\exp}$ is the time ordered exponential and $\hat{W}(t) = \mathrm{e}^{-\hat{V}_0 t/\mathrm{i}\overline{h}}\hat{W}\mathrm{e}^{\hat{V}_0 t/\mathrm{i}\overline{h}}$. For latter convenience, we introduce $\hat{u} = \int_0^1 \mathrm{d}\tau\ \hat{W}(\tau)$. Assuming that the difference between $E/\overline{h}$ and $\bar{E}/\overline{h} \equiv (f+g)/(2\overline{h})$ is $\mathcal{O}(\epsilon)$: we can consider the following expansion by ϵ:

$$\mathrm{e}^{-E/\mathrm{i}\overline{h}}\hat{U}_{\mathrm{trunc}} = \hat{1} + \frac{1}{\mathrm{i}\overline{h}}(\hat{H}_{\mathrm{trunc}} - E\hat{1}) + \mathcal{O}(\epsilon^2) \tag{A8}$$

where, by using (A5) and (A7), $\hat{H}_{\mathrm{trunc}}$ can be expressed as

$$\hat{H}_{\mathrm{trunc}} = \bar{E} + \epsilon\bar{u} + \frac{\Delta E^{\mathrm{unpert}} + \epsilon\Delta u}{2}\begin{pmatrix}1 & 0\\ 0 & -1\end{pmatrix} + \epsilon\begin{pmatrix}0 & J_{\mathrm{eff}}^*\\ J_{\mathrm{eff}} & 0\end{pmatrix}. \tag{A9}$$

Here, $\bar{u} = (\langle\phi|\hat{u}|\phi\rangle + \langle\psi|\hat{u}|\psi\rangle)/2$ is the perturbed energy shift, $\Delta u = \langle\phi|\hat{u}|\phi\rangle - \langle\psi|\hat{u}|\psi\rangle$ is the perturbed energy difference and $J_{\mathrm{eff}} = \langle\psi|\hat{u}|\phi\rangle$ is the effective tunnelling matrix element. Finally, from (A4) and (A8), the eigenvalue equation becomes

$$\hat{H}_{\mathrm{trunc}}\begin{pmatrix}\alpha\\ \beta\end{pmatrix} = \begin{pmatrix}\alpha\\ \beta\end{pmatrix}E + \mathcal{O}(\epsilon^2). \tag{A10}$$

We apply the general formula (A10) to our model system used in the main text, the spin-kicked rotor, when the coupling $B_x(\hat{q})$ between two manifolds $|\uparrow\rangle$ and $|\downarrow\rangle$ is weak. For this model, the quantities that appeared in the general analysis are expressed as $\hat{V}_0 = B_z(\hat{q})\hat{\sigma}_z$ and $\epsilon\hat{W} = B_x(\hat{q})\hat{\sigma}_x$. The unperturbed eigenstates are $|\phi\rangle = |\phi_{\mathrm{rot}}\rangle \otimes |\uparrow\rangle$ and $|\psi\rangle = |\psi_{\mathrm{rot}}\rangle \otimes |\downarrow\rangle$. Thus we have $\bar{u} = \Delta u = 0$ and

$$J_{\mathrm{eff}} = \langle\psi_{\mathrm{rot}}|T(\hat{q})|\phi_{\mathrm{rot}}\rangle \tag{A11}$$

where

$$T(q) = B_x(q)\frac{\sin\{B_z(q)/\hbar\}}{B_z(q)/\hbar}\mathrm{e}^{-\mathrm{i}B_z(q)/\hbar}. \tag{A12}$$

By solving (A10), we obtain two perturbed eigenstates. From these eigenstates, we can calculate their polarization as was explained in section 3. Then, we find that the polarization for the two eigenstates takes the following equal value:

$$P = \left(\frac{1+4|S|^2(|J_{\mathrm{eff}}|/\Delta E^{\mathrm{unpert}})^2}{1+4(|J_{\mathrm{eff}}|/\Delta E^{\mathrm{unpert}})^2}\right)^{\frac{1}{2}} \tag{A13}$$

where $S = \langle\psi_{\mathrm{rot}}|\phi_{\mathrm{rot}}\rangle$ is the overlapping integral between two unperturbed states of the rotor. This is the desired formula (5).

Finally, we show that the tunnelling matrix element J_{eff} appeared in (A13) can be expressed in a simpler form (q_{c} is the curve crossing point, see the explanation below) with good approximation when the following conditions are satisfied: (a) The semiclassical approximation on eigenstates $|\phi_{\mathrm{rot}}\rangle$ and $|\psi_{\mathrm{rot}}\rangle$ describes the rotor on the up and the down manifolds well; (b) as a function of q, $T(q)$ varies much slower than the phase of $\langle q|\phi_{\mathrm{rot}}\rangle$ and $\langle q|\psi_{\mathrm{rot}}\rangle$. Namely, the magnitude of the perturbation $B_z(q)$ is much smaller than the magnitude of the rotor's action integral. By using the condition (a), we are allowed to evaluate the overlapping integral $S = \int \mathrm{d}q\,\langle\psi_{\mathrm{rot}}|q\rangle\langle q|\phi_{\mathrm{rot}}\rangle$ with the stationary phase approximation. For the spin-kicked rotor, the stationary phase point is almost the same as the curve crossing point q_{c}, where the potential curves for $\langle\uparrow|\hat{V}(q)|\uparrow\rangle$ and $\langle\downarrow|\hat{V}(q)|\downarrow\rangle$ coincide (see Landau and Lifshitz 1977, section 90). Furthermore, condition (b) means that in evaluating the effective tunnelling matrix element $J_{\mathrm{eff}} = \int \mathrm{d}q\,\langle\psi_{\mathrm{rot}}|q\rangle T(q)\langle q|\phi_{\mathrm{rot}}\rangle$ by the stationary phase approximation, $T(q)$ can be regarded as just a constant amplitude factor and is factored out from the remaining oscillatory integral with good approximation. Hence, within the stationary phase approximation, equation $J_{\mathrm{eff}} = ST(q_c)$ holds. In the case of the present paper, conditions (a) and (b) are satisfied and moreover $T(q_{\mathrm{c}})$ becomes equal to J. We arrive at the final expression for J_{eff} as

$$J_{\mathrm{eff}} = SJ. \tag{A14}$$

Thus we have finished the derivation of (7) in the main text.

Appendix B. A semiclassical analysis of the pendulum in the rotational motion

In order to understand qualitatively the numerical result on the standard mapping in the regular rotational motion reported in section 3, here we analyse the rotational motion of the quantized pendulum, in the semiclassical region, which is described by the Hamiltonian

$$H = \tfrac{1}{2}p^2 + K\cos q \tag{B1}$$

where q and p are the position coordinate and the momentum of the pendulum, respectively. We expect that the pendulum will be good approximation for the regular standard mapping. We calculate, for the pendulum, (a) the energy difference

$$\Delta E_n^{\mathrm{unpert}}(K,\delta K) \equiv E_n(K+\delta K) - E_n(K-\delta K) \tag{B2}$$

and (b) the overlapping integral

$$S_n(K,\delta K) \equiv \langle n(K+\delta K)|n(K-\delta K)\rangle \tag{B3}$$

where $E_n(K)$ and $|n(K)\rangle$ are the nth eigenenergy and the nth eigenstate, respectively. In section 3, we numerically studied the dependences of the energy difference $\Delta E^{\mathrm{unpert}}$ and

the overlapping S on the nonlinear parameter K for the standard mapping in the regular rotational motion. Here we will obtain analytical expressions of ΔE^{unpert} and S for the pendulum and compare them with the numerical result for the standard mapping.

The plan of this appendix is as follows. First we formally obtain the semiclassical quantization condition and semiclassical eigenfunctions of the pendulum in the rotational motion. Next, by using a perturbation method for $k = \sqrt{2(K/E)/(1+(K/E))}$ (E: the energy of the pendulum), we derive analytical expressions of ΔE^{unpert} and S. We compare these expressions with the numerical data of the quantized standard mapping in the regular rotational region. Finally, we summarize this appendix.

Since we are interested in the rotational motion of the pendulum, we impose the condition $0 \leqslant K < E$ on the energy E of the pendulum. In order to treat rotational eigenstates in the position coordinate representation, we write the momentum p as a function of the energy E and the position q:

$$p = \sqrt{2E - 2K\cos q} \tag{B4}$$

where we choose the positive momentum $p > 0$. The semiclassical wavefunction $\psi(q)$ is expressed as follows (Landau and Lifshitz 1977, section 46):

$$\psi(q) \propto \frac{1}{\sqrt{p(q)}} \exp\left\{\frac{\mathrm{i}}{\hbar}\int^{q} \mathrm{d}q'\, p(q')\right\}. \tag{B5}$$

We impose the periodic boundary condition $\psi(q+2\pi) = \psi(q)$ on this wavefunction. The Bohr–Sommerfeld semiclassical quantization condition for the rotational motion is

$$\int_0^{2\pi} \mathrm{d}q\; p(q) = 2\pi n\hbar \tag{B6}$$

where n is an arbitrary integer. Since the integral in (B6) can be expressed with the complete elliptic integral of the second kind $\mathcal{E}(k) \equiv \int_0^{\pi/2} \mathrm{d}\theta \sqrt{1-k^2\sin^2\theta}$, the quantization condition becomes

$$8\sqrt{K}\frac{\mathcal{E}(k)}{k} = 2\pi n\hbar \tag{B7}$$

where the modulus $k = \sqrt{2K/(E+K)}$. We call the solution of (B7) k_n, which is the quantized modulus. Accordingly, the nth eigenenergy is $E_n = K(2/{k_n}^2 - 1)$. Once k_n is quantized, the action integral modulo $2\pi\hbar$, $I_n(q)$ can be expressed as

$$I_n(q) \equiv \int_{-\pi}^{q} \mathrm{d}q'\, p(q') \pmod{2\pi\hbar} \tag{B8}$$

$$= 4\sqrt{K}\,\mathcal{E}\left(\frac{q+\pi}{2}, k_n\right)\Big/ k_n \tag{B9}$$

where $\mathcal{E}(\varphi, k) \equiv \int_0^{\varphi} \mathrm{d}\theta \sqrt{1-k^2\sin^2\theta}$ is the elliptic integral of the second kind (when the action integral is substituted into (B5), this modulo operation has no effect). The nth eigenfunction of the pendulum $\psi_n(q)$ is written as follows:

$$\psi_n(q) = \frac{1}{2\sqrt{\mathcal{K}(k_n)}}\left(1 - {k_n}^2\cos^2\frac{q}{2}\right)^{-\frac{1}{4}} \exp\left\{\frac{\mathrm{i}}{\hbar} I_n(q)\right\} \tag{B10}$$

where $\mathcal{K}(k) \equiv \int_0^{\pi/2} \mathrm{d}\theta/\sqrt{1-k^2\sin^2\theta}$ is the complete elliptic integral of the first kind.

For these formal semiclassical expressions (B7) and (B10), we analyse them with the perturbation expansion for k^2, which is almost the same as the perturbation expansion for K. Actually, the lowest approximation yields the same eigenenergies and eigenfunctions

for the free rotor described by the Hamiltonian $H = \frac{1}{2}p^2$. Furthermore, we calculate the next order approximation. In this approximation, the elliptic integrals of the first and the second kinds are

$$\mathcal{F}(\varphi, k) \simeq \varphi + \frac{k^2}{4}(\varphi - \tfrac{1}{2}\sin 2\varphi) \tag{B11}$$

$$\mathcal{E}(\varphi, k) \simeq \varphi - \frac{k^2}{4}(\varphi - \tfrac{1}{2}\sin 2\varphi) \tag{B12}$$

respectively, and the complete elliptic integrals are $\mathcal{K}(k) \simeq (\pi/2)(1 - (k^2/4))$ and $\mathcal{E}(k) \simeq (\pi/2)(1+(k^2/4))$. We obtain the quantized modulus by solving (B7) approximately and the result is $k_n = (\sqrt{(\bar{h}n)^2 + 4K} - \bar{h}n)/\sqrt{K}$. Accordingly, the eigenenergy E_n and the action $I_n(q)$ for the nth eigenstate is

$$\begin{aligned} E_n &= \tfrac{1}{4}(\bar{h}n)^2 + \tfrac{1}{4}(\bar{h}n)\sqrt{(\bar{h}n)^2 + 4K} - \tfrac{1}{2}K \\ &= \tfrac{1}{2}(\bar{h}n)^2 + \mathcal{O}(K^2) \end{aligned} \tag{B13}$$

$$\begin{aligned} I_n(q) &= \bar{h}n(q + \pi) - \tfrac{1}{2}\left(\sqrt{(\bar{h}n)^2 + 4K} - \bar{h}n\right)\sin q \\ &= \bar{h}n(q + \pi) - \frac{\sin q}{\bar{h}n}K + \mathcal{O}(K^2). \end{aligned} \tag{B14}$$

The eigenfunction of the nth state $\psi_n(q)$ becomes

$$\psi_n(q) = \frac{1}{\sqrt{2\pi}}(1 + \tfrac{1}{8}{k_n}^2\cos q)\exp\left\{\frac{\mathrm{i}}{\bar{h}}I_n(q)\right\}. \tag{B15}$$

Let us proceed to calculate the energy difference $\Delta E_n^{\mathrm{unpert}}$ (B2). Though we have obtained the approximate expression (B13) for $E_n(K)$, we cannot utilize directly this expression (B13) to calculate $\Delta E_n^{\mathrm{unpert}}$ through (B2), since the approximate expression (B13) for $E_n(K)$ does not depend on K due to the low order of the approximation. Instead, we expand $\Delta E_n^{\mathrm{unpert}}$ by small δK:

$$\Delta E_n^{\mathrm{unpert}} = \frac{\partial E_n(K)}{\partial K}(2\delta K) + \mathcal{O}(\delta K^2) \tag{B16}$$

and evaluate $\partial E_n/\partial K$ semiclassically below. The derivative $\partial E_n/\partial K$ can be expressed as

$$\frac{\partial E_n(K)}{\partial K} = \langle n(K)|\cos\hat{q}|n(K)\rangle. \tag{B17}$$

Then, with (B16), (B17), (B15) and (B14), we obtain the final expression for $\Delta E_n^{\mathrm{unpert}}$

$$\Delta E_n^{\mathrm{unpert}} = \frac{1}{4}\frac{K}{E_n}\left(1 + \frac{K}{E_n}\right)^{-1}(2\delta K) + \mathcal{O}(\delta K^2). \tag{B18}$$

Next, we calculate the overlapping integral S_n (B3). This can be done straightforwardly with (B15) and (B14):

$$S_n = J_0\left(\frac{1}{\bar{h}}\frac{2\delta K}{\sqrt{2E_n^0 + 4K}}\right) \tag{B19}$$

where J_0 is the Bessel function and $E_n^0 = \frac{1}{2}(\bar{h}n)^2 (\sim E_n)$.

Before closing this appendix, we compare the analytical expressions (B18) and (B19) for $\Delta E_n^{\mathrm{unpert}}$ and S_n, which are derived for the quantized pendulum, with the corresponding numerical experiments performed for the quantized standard mapping. In the numerical experiments, the nonlinear parameter K is taken to be 0.4 or 0.8 to realize the regular

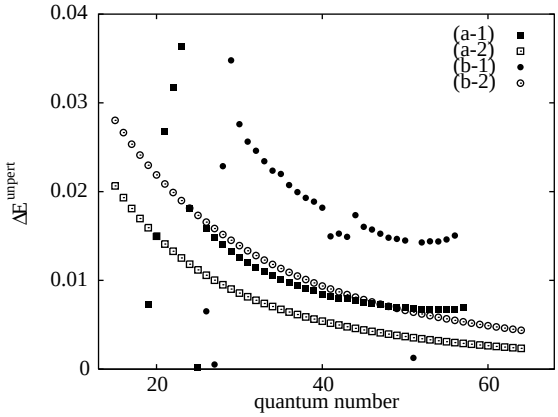

Figure B1. Quantum number n dependences of $\Delta E^{\rm unpert}$. The semiclassical theory of the pendulum and the numerical result of the standard mappings corresponds to (1) and (2), respectively. The values of the nonlinear parameter K are (a) $K = 0.4$, (b) $K = 0.8$. Other parameters are $h/(2\pi)^2 = 0.007\,816$ and $\delta K = 0.0625$.

motion and the rotational eigenstates around $2\pi/3 \lesssim p \lesssim \pi$ are considered. Common parameters are $\delta K = 0.0625$ and $h/(2\pi)^2 = 0.007\,816$.

First, let us consider the energy difference $\Delta E^{\rm unpert}$. In order to compare the semiclassical expression (B18) of the pendulum and the numerical result of the standard mappings, we show the quantum number n dependencies of $\Delta E^{\rm unpert}$ in figure B1. The scatter around $20 \lesssim n \lesssim 30$ is caused by the resonance located at $p = 0$. At the same time, since the region that has larger quantum number ($\sim$50) corresponds to the resonance located at $p = \pi$, we do not show the data in the region. The difference between the pendulum and the standard mapping is a factor of 2–3. This is due to the absence of the higher order nonlinear resonances in the pendulum, especially the 1:2 resonance located at $(q, p) = (0, \pi), (\pi, \pi)$, which has a large influence on the phase-space dynamics of the standard mapping even in the regular region $K < K_c$. Except for this discrepancy in absolute magnitudes, the proportionality of ΔE to K with positive coefficient, which was derived for the pendulum by the perturbation expansions (B18), is actually observed for the standard mapping. The reason why $\Delta E^{\rm unpert}$ becomes larger for increased K can be explained intuitively as follows. Since $\mathrm{d}(\Delta E_n^{\rm unpert})/\mathrm{d}K \cong 2\delta K\, \mathrm{d}(\langle n(K)|\cos\hat{q}|n(K)\rangle)/\mathrm{d}K$ from (B16) and (B17), we have to explain that the averaged potential $\langle n(K)|\cos\hat{q}|n(K)\rangle$ over the nth rotational state takes larger value for increased K. However, this is simple. When K is increased, the eigenenergy $E_n(K)$, which is the total energy of the corresponding motion in the semiclassical theory, can be regarded as almost a constant since $E_n(K) = E_n(0) + \mathcal{O}(K^2)$; on the other hand, the potential energy $K\cos q$ takes a larger magnitude due to the trivial linear dependence on K. Accordingly, around $q \approx 0$ or 2π where the potential $K\cos q$ takes its maximum value, the kinetic energy, which is the difference between the total energy and the potential energy, of the classical motion corresponding to the nth eigenstate, takes a smaller value closer to zero for the increased K. The small kinetic energy around $q \approx 0$ or 2π means the slow velocity and the longer stay time there. Consequently, large positive values of the potential $K\cos q$ around $q \approx 0$ or 2π is emphasized in evaluating $\langle n(K)|\cos\hat{q}|n(K)\rangle$ semiclassically and this quantity takes a larger value.

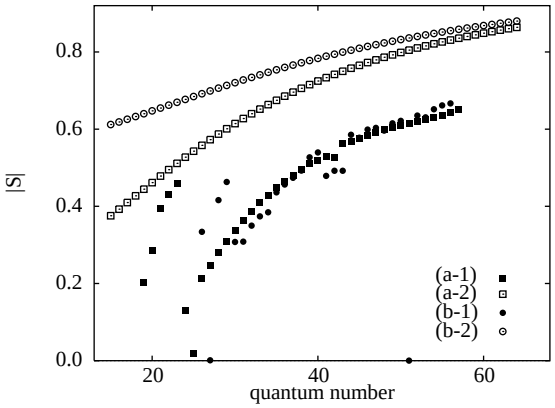

Figure B2. Quantum number n dependences of $|S|$. Others are the same as in figure B1.

Next we consider the overlapping $|S|$. In figure B2, we show the quantum number dependences of $|S|$ calculated by the semiclassical theory of the pendulum (B19) and the numerical result of the standard mappings. The semiclassical result (B19) overestimates the values of $|S|$ by 40% compared to the numerical result of the standard mappings. The reason for the difference between these two systems is the same as in the case of the energy difference which is mentioned above. On the other hand, the weak dependence of S on K is common to the standard mapping and the pendulum. This weak dependence of S on K originates from the fact $S(K = 0) \neq 0$. In this aspect, the overlapping integral S contrasts sharply with the energy difference $\Delta E_n^{\text{unpert}}$, for which the vanishing value $\Delta E_n^{\text{unpert}} = 0$ at $K = 0$ results in a strong dependence of $\Delta E_n^{\text{unpert}}$ on K around $K = 0$.

We summarize this appendix. First, we analysed the quantized pendulum in regular rotational motion. For the energy difference ΔE^{unpert}, we obtained the K dependence $\Delta E_n^{\text{unpert}} = CK, C > 0$ for small K (B18). On the other hand, the overlapping integral S_n depends on K only weakly (equation (B19)). Next we compared these results for the pendulum with the behaviour of the quantized standard mapping. Although the agreement is only qualitatively, our analysis for the pendulum explains the K dependences of ΔE^{unpert} and S of the quantized standard mapping in the regular rotational motion.

References

Bohigas O, Tomsovic S and Ullmo D 1993 *Phys. Rep.* **223** 43
Brillouin L 1926 *J. Phys. Radium* **7** 353
Casati G, Chirikov B V, Izrarelev F M and Ford J 1979 *Lecture Notes in Physics* **93** 334
Chirikov B V 1979 *Phys. Rep.* **52** 263
Einstein A 1917 *Verh. Dtsch. Phys. Ges.* **19** 82
Espagnat B d 1976 *Conceptual Foundations of Quantum Mechanics* (MA: Benjamin)
Feynman R P, Vernon F L and Hellwarth R W 1957 *J. Appl. Phys.* **28** 49
Fishman S, Grempel D R, and Prange R E 1982 *Phys. Rev. Lett.* **49** 509
Gutzwiller M C 1990 *Chaos in Classical and Quantum Mechanics* (New York: Springer)
Holstein T 1959 *Ann. Phys.* **8** 343
Hushimi K 1940 *Proc. Phys. Math. Soc. Japan.* **22** 264
Kagan Yu and Kilnger M I 1974 *J. Phys. C: Solid State Phys.* **7** 2791
Keller J B 1958 *Ann. Phys.* **4** 180
Landau L D and Lifshitz E M 1977 *Quantum Mechanics (Non-relativistic Theory)* (New York: Oxford University Press)

Lichtenberg A J and Lieberman M A 1992 *Regular and Chaotic Dynamics* (New York: Springer)
Roncaglia R, Bonci L, Izrailev F M, West B J and Grigolini P 1994 *Phys. Rev. Lett.* **73** 802
Scharf R 1989 *J. Phys. A: Math. Gen.* **22** 4223
Shepelyansky D L 1986 *Phys. Rev. Lett.* **56** 677
Shudo A and Ikeda K S 1995 *Phys. Rev. Lett.* **74** 682
Takahashi K and Saitô N 1985 *Phys. Rev. Lett.* **55** 645
Toda M and Ikeda K 1987 *J. Phys. A: Math. Gen.* **20** 3833
Tomsovic S and Ullmo D 1994 *Phys. Rev.* E **50** 145
Utermann R, Dittrich T and Hänggi P 1994 *Phys. Rev.* E **49** 273
Zurek W H 1982 *Phys. Rev.* D **26** 1862